

Electronic supplementary information for

**Coaxial Cu-Si@C array electrodes for high-performance
lithium ion batteries**

Hasigaowa Guan, Xi Wang, Shimou Chen, Yoshio Bando, and Dmitri Golberg

Experimental

Synthesis of coaxial Cu-Si@C arrays: First step is the synthesis of Cu nanorod arrays. One side of an AAO template was coated with a thin layer of Pt to serve as a working electrode by using a LEICA EM SCD500 High Vacuum Sputter Coater. Also the presence of Pt film can prevent the coaxial hybrid structures from collapsing after the removal of templates. Electrodeposition of Cu was performed in a three-electrode, single compartment electrochemical cell at 25 °C. The electrolyte solution was 10 g/L CuSO₄ and 30 g/L (NH₄)₂SO₄. Electrodeposition of Cu was performed at a constant potential of 0.8 V versus saturated calomel reference electrode (SCE) by using Cu foil as a counter electrode in solution. After 2 h, Cu was filled into AAO, and then Cu nanorod arrays was obtained followed by dissolving the template in 3 M NaOH solution for 1 h. Secondly, the growth of Si@C layers onto the surface of Cu nanopillars was performed by using chemical vapor deposition. Then Cu arrays were placed in the tubular furnace, and the boat filled with the prepared butyl-capped Si gels was placed in the furnace. It was heated to 850 °C in an argon flow (100 sccm) for 1 h and then the furnace was cooled to room temperature in Ar flow. Finally, the sample was plasma etched for 1 h (Ar buffer gas, 100 W, 5 Pa) by using a reaction ion etching system (L-451D-L, ANELVA) in order to remove an amorphous Si-carbon layer formed in the process of chemical vapor deposition.

Characterization. X-ray powder diffraction (XRD) patterns were recorded on a Philips X'Pert PRO MPD X-ray diffractometer operated at 35 kV and 45 mA with Cu K α radiation. Transmission electron microscopy (TEM) images were taken on a JEOL JEM-3000F transmission electron microscope with an accelerating voltage of 300 kV. FE-SEM analysis was carried out using a field-emission microscope (JEOL S-F4800) operated at 10 kV.

Electrochemical Characterization: The electrochemical properties of samples

were measured with three-electrode cells. Li metal foil was selected as the reference and counter electrode. The electrolyte was 1 M LiClO₄ in ethyl carbonate (EC) and diethyl carbonate (DEC) (EC : DEC = 1 : 1 in v/v). The cells were assembled in a glove box filled with pure argon gas. Galvanostatic discharge/charge measurements were performed in a potential range of 2 V-0.05 V vs Li⁺/Li. The specific capacity of the Cu-Si@C composite was calculated based on the weight of Si@C, which was determined by subtracting the weight of Cu from the overall weight of Cu-Si@C arrays.

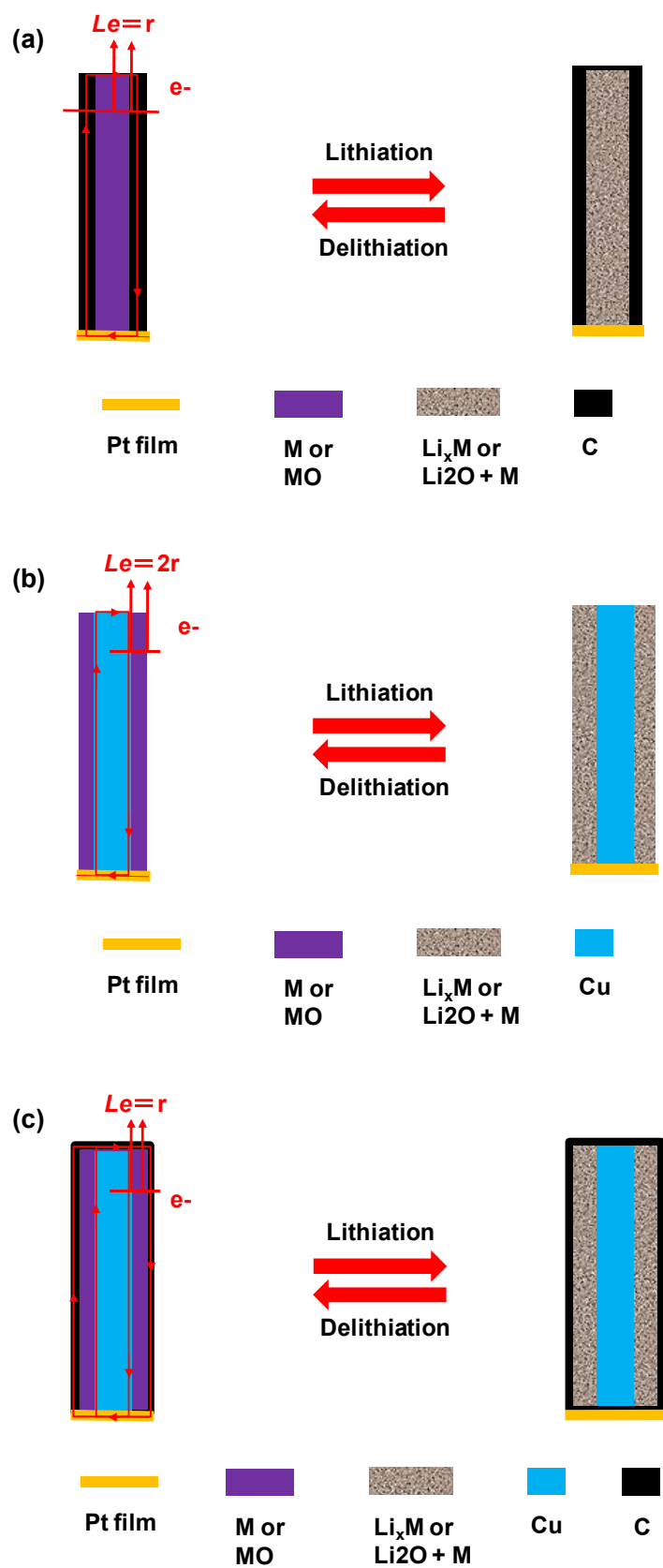


Fig. S1 Schematic illustration of the electronic transport length (L_e) and morphology changes during a lithiation-delithiation process in three types of

electrodes: (a) active material-core/conductive material-shell (type I), (b) conductive material-core/active material-shell (type II), (c) robust conductive material (here Cu)/ active material/ thin elastic electroconductive layer (carbon shell) (type III).

We supposed that the thickness of active materials in three cases is the same, and was denoted as $2r$. It is well-known that the transport of electrons in electrode active materials plays the similarly important role as the lithium-ion intercalation/de-intercalation.¹⁻³ Unfortunately, most of the electrode active materials are semiconductors or insulators. The large resistance arising from the low electronic conductivity and the boundary interfaces would largely hinder the high power performance of lithium-ion batteries. In cases of type I and type III shown in Fig. S1a and Fig. S1c, the active materials are covered by the conductive layers; in contrast, there is only one side of active materials contacted with the conductive materials in the case of type II. Therefore, it is obvious that the electronic transport length (L_e) in type III is smaller than that of types I and II. That is, there is a structural benefit in the architecture of type III compared with the types I and II. Secondly, the main disadvantage that restricts the application of anode materials is the large volume changes (>200%) during Li^+ insertion and extraction, which results in a pulverization of the electrodes and peeling off the current connection network, and thus a rapid capacity decline upon cycling. To overcome this issue, type I and type II electrodes have been designed. Owing to the lack of effective protection, the active materials located on the surface of robust conductive core would become amorphous structures and thus would gradually be peeled off from the surface, thus leading to a fast loss in the capacity upon multiple cycling. In our designed type III, the active materials are tightly sandwiched between the robust conductive materials and the elastic carbon layers. Being a conductive coat which covers the active materials, both the robust core

and the outer elastic shell not only ensure a continuous contact, but also buffer the volume changes of active particles upon lithium-ion insertion/extraction, thus affording a much better cycle performance during a long term charge/discharge. In this three layered electrode, the elastic conductive material, carbon, is generally designed as the outer coating layer because it can effectively buffer the volume variation during the lithiation and delithiation; while the robust conductive material, such as Cu, is commonly selected as the inner core. Such structure not only allows for effective electron conduction to enhance the battery's high rate performance but also provides structural reinforcement to overcome the mechanical rupture during the volume changes of anodes.

1 Y. Wang, H. Li, P. He, E. Hosono, H. Zhou, *Nanoscale*. **2010**, *2*, 1294.

2 A. S. Aricò, P. G. Bruce, B. Scrosati, J. -M. Tarascon, W. V. Schalkwijk, *Nat. Mater.* **2005**, *4*, 366.

3 Y. G. Guo, J. S. Hu, L. J. Wan, *Adv. Mater.* **2008**, *20*, 2878.

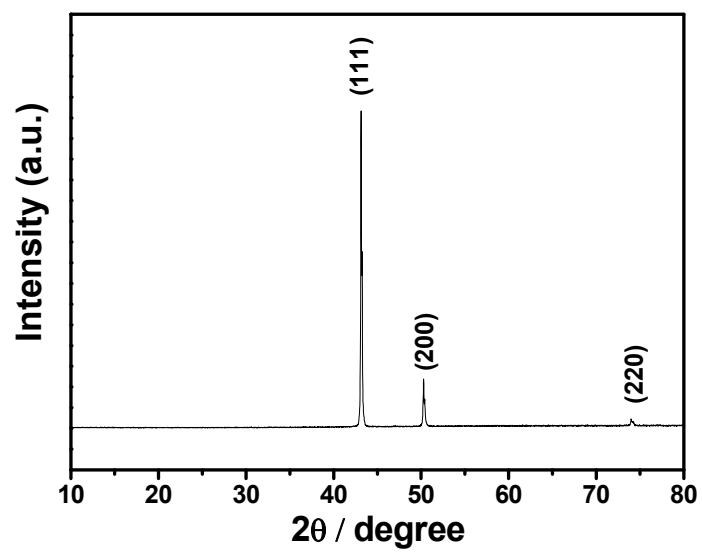


Fig. S2 XRD pattern of Cu-Si@C arrays.

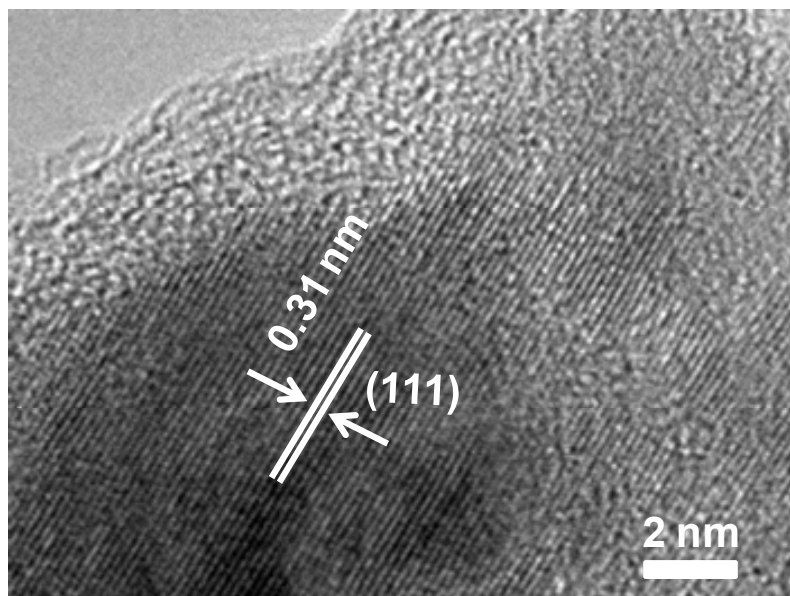


Fig. S3 Representative HRTEM image of the shell of a Cu-Si@C nanorod.

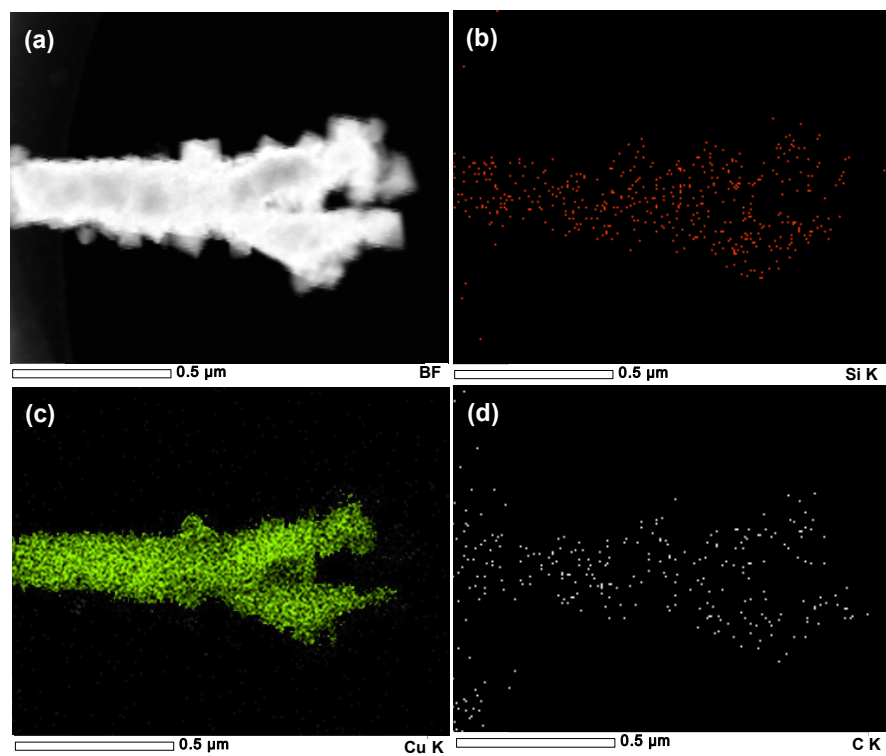


Fig. S4 (a) Dark-field TEM image of a single Cu-Si@C nanorod, and (b-d) The corresponding elemental maps of the nanorod: Si, Cu, and C EDX maps.

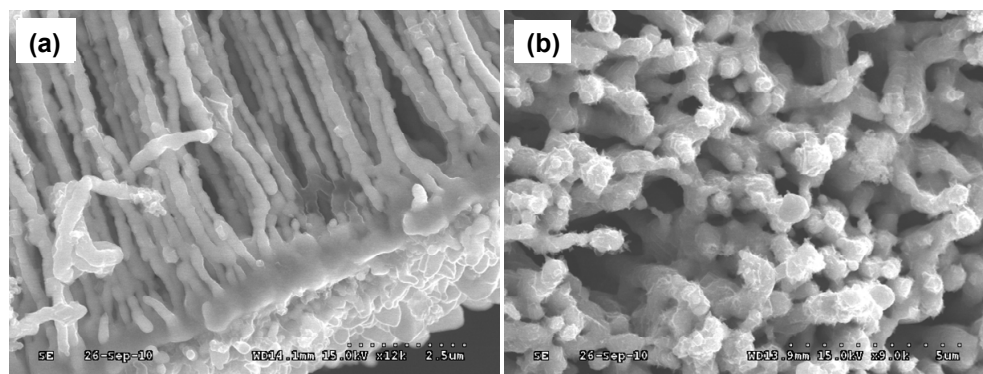


Fig.S5 SEM characterizations of the coaxial Cu-Si@C arrays in a fully delithiated state after 50 discharge/charge cycles: (a) the bottom section, and (b) the top part.